ISSN 0036-0244, Russian Journal of Physical Chemistry A, 2021, Vol. 95, Suppl. 2, pp. S288–S295. © Pleiades Publishing, Ltd., 2021.

STRUCTURE OF MATTER AND QUANTUM CHEMISTRY

# Facile Synthesis of Cobalt Tungstate with Special Defect Structure with Enhanced Optical, Photoluminescence, and Supercapacitive Performances

**Huajing Gao[a,b], Shengnan Tang[a], Xiangyu Chen[a], Chuan Yu[a], Shifa Wang[a,c,d,*], Leiming Fang[d,**], Xianlun Yu[a], Xinxin Zhao[a], Guangzhuang Sun[a], and Hua Yang[b]**

[a] *School of Electronic and Information Engineering, Chongqing Three Gorges University, Chongqing, Wanzhou, 404000 China*

[b] *School of Science, Lanzhou University of Technology, Lanzhou, 730050 China*

[c] *Chongqing Key Laboratory of Geological Environment Monitoring and Disaster Early-warning in Three Gorges Reservoir Area, Chongqing Three Gorges University, Chongqing, Wanzhou, 404000 China*

[d] *Institute of Nuclear Physics and Chemistry, China Academy of Engineering Physics, Sichuan, Mianyang, 621900 China*

** e-mail: wangshifa2006@yeah.net*

*** e-mail: flmyaya2008@163.com*

Received October 29, 2020; revised October 29, 2020; accepted November 4, 2020

**Abstract**—The present study reports the gamma-ray irradiation assisted polyacrylamide gel synthesis and optical, photoluminescence and supercapacitive performances of cobalt tungstates with special defect structure. The analysis of X-ray powder diffraction data showed that the purity and crystallinity of $CoWO_4$ increased with the increasing of sintering temperature. X-ray photoelectron spectroscopy and energy spectrum analysis show that the high purity $CoWO_4$ powders does not contain any other impurities. Color and optical properties analysis indicates that the high purity $CoWO_4$ powders exhibits a strongest blue color than that of other samples. The photoluminescence spectrum shows three obvious emission bands in ultraviolet (340–375 nm), blue (424–490 nm), and green light emission (510 nm) regions under 220 nm xenon lamp excitation, which are ascribed to the organic impurities, the transition of $^3T_{1u}$ levels to the $^1A_{1g}$ level, and the partially allowed transition of $T_{1g}$ to $^1A_{1g}$, respectively. Studies on electrochemical properties demonstrate that the $CoWO_4$ powder has an excellent prospect in the supercapacitors for advanced electrochemical energy storage applications.

**Keywords:** $CoWO_4$, sintering temperature, optical properties, emission band, blue light emission, supercapacitor

**DOI:** 10.1134/S0036024421150103

## INTRODUCTION

With the development of market economy, the demand for semiconductor luminescent materials is increasing day by day. However, traditional luminescent materials are difficult to meet the rapid economic development and market demand. Various new methods for improving luminescent materials have been developed, mainly including: (1) rare earth ion doping activates luminescent materials [1–6]; (2) composite of multi-component single-phase luminescent materials [7–13]; (3) construct luminescent materials with special defect structures [14]. In these methods, the construction of special defect structure does not introduce other impurity elements or semiconductor materials, which is favored by researchers.

Cobalt tungstate is a highly efficient self-activated luminescent material, which has potential applications in luminescent devices, flat panel display and lighting system outside the space station window [15–17]. Due to the high energy band value of $CoWO_4$ and the low recombination rate of electrons and holes, its luminous efficiency is low and it is difficult to be applied industrially. In recent years, γ-ray irradiation assisted polyacrylamide gel method (GIAPGM) can enhance the physical and chemical properties of single-phase materials by making them have special defect structure without introducing any impurity [18, 19]. Therefore, it is of great significance to synthesize $CoWO_4$ phosphor with special defect structure by using GIAPGM and to study its optical, photoluminescence and supercapacitor properties.

In this paper, we propose the synthesis of $CoWO_4$ phosphor with special defective structure by GIAPGM. The effects of sintering temperature on phase purity, crystallinity, functional group, optical, photoluminescence and supercapacitor properties of

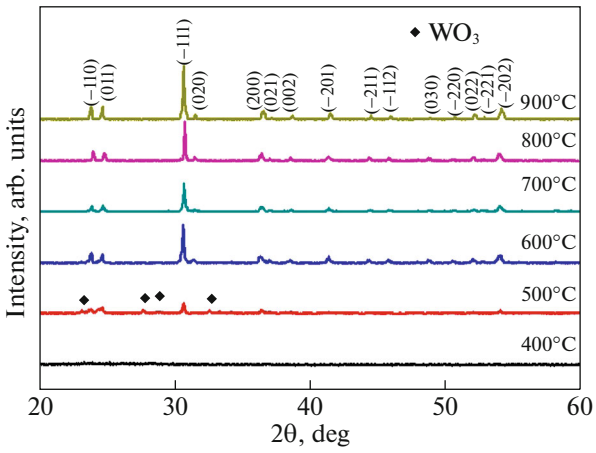


**Fig. 1.** XRD patterns of samples S1, S2, S3, S4, S5, and S6.

$CoWO_4$ phosphors have been studied systematically. Reasons for enhancement of photoluminescence emission intensity of $CoWO_4$ phosphors with special defect structure are discussed in detail. The $CoWO_4$ phosphor was used as a electrode material and its electrochemical performances were studied by electrochemical impedance spectroscopy technology, cyclic voltammetry, and galvanostatic charge/discharge.

## EXPERIMENTAL

### *Synthesis of $CoWO_4$ Phosphors*

$CoWO_4$ phosphors were prepared by GIAPGM with cobalt chloride and tungstic acid used as metal source [20, 21]. 0.015 mol/L cobalt chloride and tungstic acid with molar ratio $n_{Co} : n_W = 1 : 1$, 4.7282 g citric acid, 20 g glucose, 9.5958 g acrylamide, and 1.9192 g *N*,*N*'-methylene diacrylamide were dissolved in turn in 100 mL deionized water. The above experimental process is completed under magnetic agitation. After the above reagent is completely dissolved, it is transferred to a sealed glass bottle for 20 kGy γ-ray irradiation to obtain gel. The gel is then dried at 120°C in a drying oven for 24 h. Subsequently, the xerogel powder sintered at 400, 500, 600, 700, 800, and 900°C for 5 h to obtain $CoWO_4$ phosphors are labeled as samples S1, S2, S3, S4, S5, and S6.

### *Material Characterization*

The phase purity, crystallinity, and functional group of samples S1, S2, S3, S4, S5, and S6 were recorded by a DX-2007BH X-ray diffractometer (XRD). The charge state of sample S6 was characterized by a KRATOS X SAM 800 X-ray photoelectron spectrometer. The surface morphology of sample S6 was characterized by scanning electron microscopy (SEM) and transmission electron microscopy (TEM). Ultraviolet–visible (UV–Vis) diffuse reflectance spectra of samples S1, S2, S3, S4, S5, and S6 were measured by a UV1800 UV–Vis spectrophotometer with a integrating sphere as a attachment. The photoluminescence (PL) properties of samples S1, S2, S3, S4, S5, and S6 were studied by a SHIMADZU RF-5301PC fluorescence spectrophotometer. The electrochemical properties of samples S1, S2, S3, S4, S5, and S6 were investigated on a CST 350 electrochemical workstation through using a three-electrode cell as described in the previous reports [22, 23].

## RESULTS AND DISCUSSION

### *Phase Purity and Structure Analysis*

To study the effect of sintering temperature on the phase transition of $CoWO_4$ xerogel, XRD is used to detect the phase purity and structure of $CoWO_4$ samples. Figure 1 shows the XRD patterns of samples S1, S2, S3, S4, S5, and S6. An amorphous state can be observed for the sample S1. With the sintering temperature rising to 500°C, the diffraction peaks of $CoWO_4$ with standard JCPDS card no. 15-0867 and $WO_3$ with standard JCPDS card no. 20-1324 appeared in the sample. When the temperature continues to rise, the diffraction peak of $WO_3$ disappears, leaving only the diffraction peak of $CoWO_4$. With the increase of sintering temperature, the intensity of $CoWO_4$ diffraction peaks increases continuously. From the XRD results, it can be inferred that at low temperature, $H_2WO_4$ is firstly decomposed into $WO_3$ and $H_2O$, and then $WO_3$ reacts with Co ions in the precursor to produce $CoWO_4$

$$H_2WO_4 \rightarrow WO_3 + H_2O, \quad (1)$$

$$2WO_3 + 2Co^{2+} + O_2 \rightarrow 2CoWO_4. \quad (2)$$

### *XPS Analysis*

XPS technology can be used to detect any impurities contained in a sample. In order to study the chemical composition and oxidation state of $CoWO_4$, XPS was used to measure the sample S6, as shown in Fig. 2. The survey spectra of sample S6 exhibits the characteristic peaks of C, O, Co, and W elements in the range of 0–1350 eV as shown in Fig. 2a. Although the characteristic peak of element C can be observed in the sample, it is mainly caused by the calibration peak of XPS instrument, so $CoWO_4$ sample does not contain any impurities. [22, 23]. Figure 2b shows the Co 2*p* electron level of sample S6. The two characteristic peaks at 779.21 and 795.32 eV are assigned to $Co^{3+}$ ions and the satellite peaks at 7861.90 and 800.52 eV are ascribed to $Co^{2+}$ ions [16]. Due to the presence of Co vacancy, charge compensation will occur in W ion, which will affect the photoluminescence performance of $CoWO_4$ [24]. The W 4*f* electron level of sample S6 as shown in Fig. 2c. According to the literature [25],

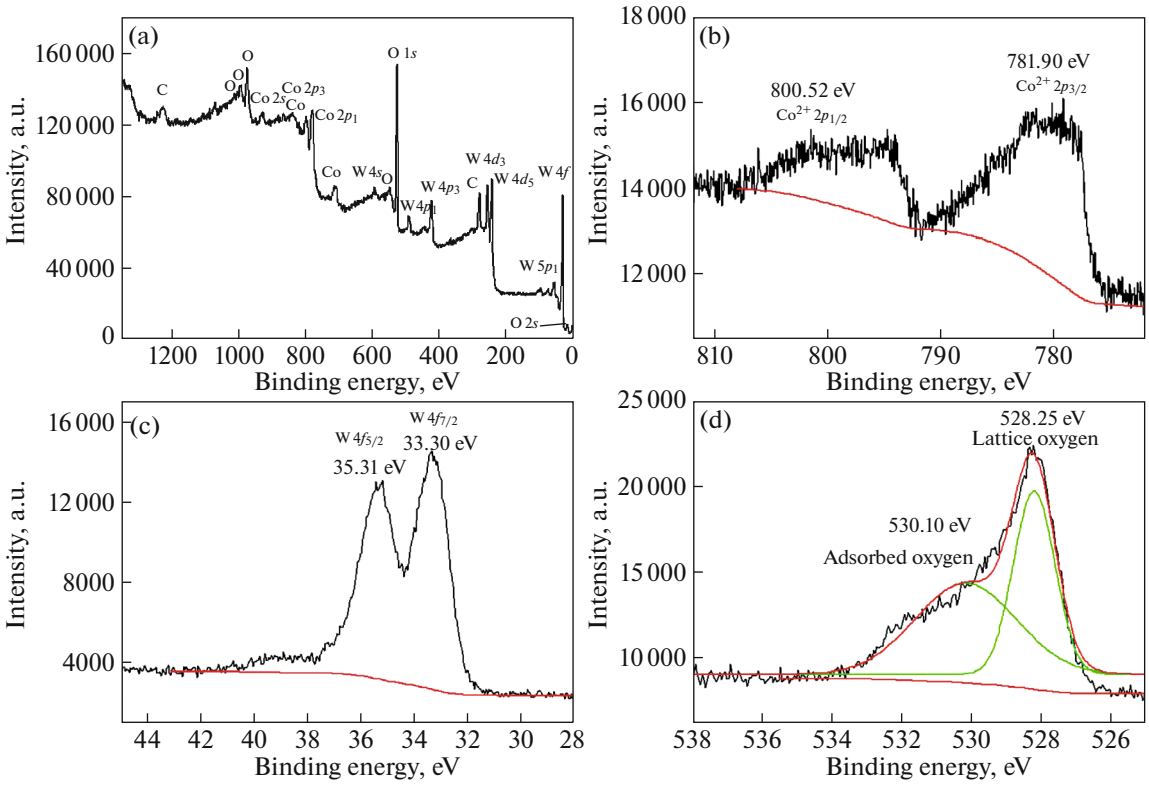


**Fig. 2.** XPS spectra of sample S6: (a) survey spectra, (b) Co 2*p* electron level, (c) W 4*f* electron level, and (d) O 1*s* electron level.

the characteristic peaks of W $4f_{5/2}$ and W $4f_{7/2}$ were observed around 38 and 36 eV, respectively for the pure $WO_3$. In this experiment, the characteristic peaks of W $4f_{5/2}$ and W $4f_{7/2}$ are significantly displacement, indicating that $CoWO_4$ is formed. The O 1*s* electron level of sample S6 as shown in Fig. 2d. The two characteristic peaks at 530.10 and 528.25 eV can be assigned to adsorbed oxygen [26] and lattice oxygen, [27] respectively. The results show that the $CoWO_4$ synthesized by GIAPGM has high surface adsorbed oxygen and Co vacancy, suggesting that the material has excellent photoluminescence properties.

### *Surface Morphology*

Surface morphologies observed by SEM and TEM for the sample S6. Figure 3a shows the SEM image of sample S6. The image show that the $CoWO_4$ particle formation is fine, the particle boundaries are distinct and the particle surface appears quite smooth for the $CoWO_4$ sample. The particles appear to grow up and become rice grains. The average diameter is about 300 nm. The element composition of sample S6 was further characterized by EDS spectra as shown in Fig. 3b. The major elements for the sample S6 are C, O, W, Co, and Cu. The characteristic peaks of C and Cu elements are ascribed to the TEM microgrid. The results also indicate that there are no other impurity elements in the sample S6. Figure 3c shows the TEM image of sample S6. The average diameter of particles is consistent with the SEM observation results. Figure 3d shows the HRTEM image of $CoWO_4$ products. The lattice spacing of 0.3597 and 0.2915 nm corresponds to the *d*-spacing of (112) and (−111) planes, respectively. The (112) and (−111) planes can be assigned to the $CoWO_4$ with the standard JCPDS card no. 15-0867. The result indicates that the $CoWO_4$ grains grew along the (112) and (−111) planes.

### *Optical Properties*

UV–Vis diffuse reflectance spectroscopy can be used to analyze the color properties of semiconductor materials. The UV–Vis diffuse reflectance spectra of samples S1, S2, S3, S4, S5, and S6 as shown in Fig. 4a. Four obvious diffuse peaks at 250, 460, 520, and 680 nm were observed for the samples S1, S2, S3, S4, S5, and S6. The color-related parameters includes ($L^*$, $a^*$, $b^*$), the hue angle ($H°$), the chroma parameter ($c^*$), and the total colour difference ($\Delta E^*_{CIE}$) can be calculated by previous reports [28] and following equations:

$$H° = \arctan\left(\frac{b^*}{a^*}\right), \quad (3)$$

$$\Delta E^*_{CIE} = \sqrt{(L^*)^2 + (a^*)^2 + (b^*)^2}, \quad (4)$$

$$c^* = \sqrt{(a^*)^2 + (b^*)^2}. \quad (5)$$

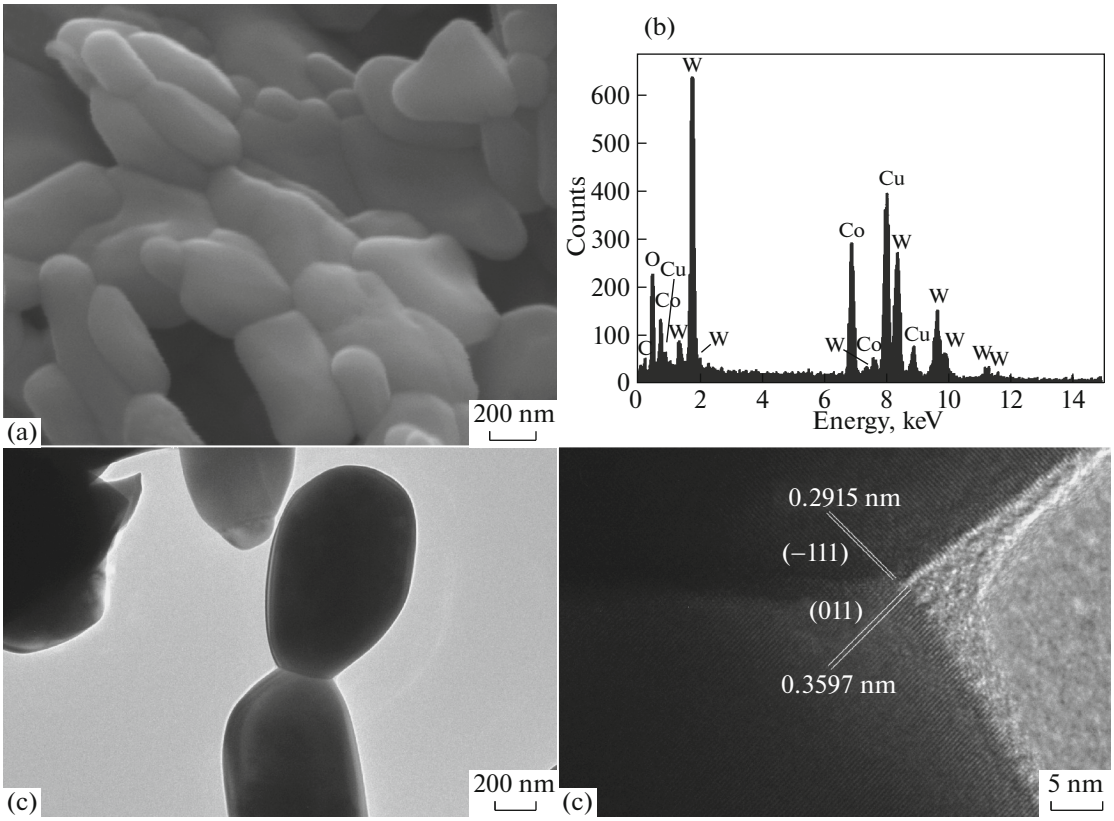


**Fig. 3.** (a) SEM image, (b) EDS, (c) TEM and (d) HRTEM image of sample S6.

Table 1 shows the color coordinates of samples S1, S2, S3, S4, S5, and S6. Generally, the blue component of the sample is determined by the parameters of $b^*$, with more negative $b^*$ value means more obvious blue. The result indicates the blue component of sample S6 is better than other samples. In the temperature range of 700–900°C, the absolute value of $a^*$, $b^*$, $c^*$ increases with the increasing of sintering temperature, suggesting that the crystallinity of $CoWO_4$ increases with the increasing of sintering temperature.

The UV–Vis absorption spectrum of samples S1, S2, S3, S4, S5, and S6 are calculated on the basis of UV–Vis diffuse reflectance spectra and K–M theory:

$$F(R) = \frac{\alpha}{S} = \frac{(1 - R_\infty)^2}{2R}, \quad (6)$$

where $S$ is the scattering coefficient, $\alpha$ is the absorption coefficient, and $R$ is the reflectance. The UV–Vis absorption spectrum of samples S1, S2, S3, S4, S5, and S6 as shown in Fig. 4b. Five obvious absorption peaks at 206, 330, 520, 585, and 785 nm were observed for the samples S1, S2, S3, S4, S5, and S6. The absorption peaks at (206, 330), (520, 585), and 785 nm can be assigned to the $[WO_6]^{6-}$ complex within the wolframite structure, the $d$–$d$ transition band and Co vacancy, respectively [8, 29]. The reason why the absorption coefficient of sample S1 is inconsistent

**Table 1.** Color coordinates and $E_g$ values of samples S1, S2, S3, S4, S5, and S6

| Sample | Color coordinates | | | | | | $E_g$, eV |
|---|---|---|---|---|---|---|---|
| | $L^*$ | $a^*$ | $b^*$ | $c^*$ | $H^o$ | $\Delta E^*_{CIE}$ | |
| S1 | 77.610 | –0.101 | 0.450 | 0.461 | –77.350 | 77.611 | 5.176 |
| S2 | 46.761 | –0.289 | –1.171 | 1.206 | 76.137 | 46.777 | 4.760 |
| S3 | 71.240 | –4.578 | –5.875 | 7.448 | 52.073 | 71.628 | 4.885 |
| S4 | 83.695 | –3.451 | –3.996 | 5.280 | 49.186 | 83.861 | 5.152 |
| S5 | 84.049 | –3.505 | –5.228 | 6.294 | 56.161 | 84.284 | 5.191 |
| S6 | 78.193 | –3.600 | –7.350 | 8.184 | 63.905 | 78.620 | 5.105 |

with other samples may be that the sample contains a large number of organic impurities.

The optical band gap ($E_g$) values of samples S1, S2, S3, S4, S5, and S6 by the Tauc relation:

$$(F(R)h\nu)^n = A(h\nu - E_g), \quad (7)$$

where $F(R) = \alpha$, $h\nu$ is the photon energy, and $A$ is a constant. The $E_g$ values of samples S1, S2, S3, S4, S5, and S6 are given Table 1. The $E_g$ values of samples S1, S2, S3, S4, S5, and S6 is found to be 5.176, 4.760, 4.885, 5.152, 5.191, and 5.105 eV, respectively. The determination of $E_g$ value of $CoWO_4$ semiconductor is conducive to the subsequent analysis of its photoluminescence mechanism.

### *Photoluminescence Properties*

Figure 5 shows the emission spectrum of samples S1, S2, S3, S4, S5, and S6 with the excitation wavelength at 220 nm. For the sample S1, four emission peaks at 340, 365, 424, and 470 nm can be found as shown in Fig. 5a. With the increase of sintering temperature, the intensity of emission peak in the ultraviolet region decreases or shifts until the sintering temperature is 600°C (Figs. 5a–5c), and then the emission peak in this region disappears. Combined with XRD and FTIR analysis, the emission peaks in the UV region including 340, 365, and 375 nm can be attributed to organic impurities. As the temperature increases from 400 to 500°C, the intensity of emission peak at 424 nm decreases. Therefore, the emission peak at 424 nm can be assigned to $WO_3$. At the same time, the emission peak of 510 nm can be observed when the sintering temperature reaches 600°C. The emission peaks at 465, 470, 480, 490, and 510 nm can be ascribed to $[WO_6]^{6-}$ complexes [8, 30]. When the sintering temperature reaches 700°C, the emission peak of 490 nm appears as shown in Fig. 5d. With the increase of sintering temperature, the intensity of emission peak at 490 nm also increases and blue shift occurs to 480 nm (Fig. 5f). In addition, the emission peak of 510 nm is redshifted with the increase of sintering temperature. The redshift phenomenon can be attributed to the presence of adsorbed oxygen on the $CoWO_4$ surface. In Fig. 5f, the emission peak at 440 nm can be assigned to the scattering peak.

With the increase of sintering temperature, the emission intensity first decreases, then increases and then decreases. The first reduction may be due to a reduction in the amount of organic impurities in the sample. In addition, the appearance of $WO_3$ also weakens the emission intensity of samples. The second reduction was mainly due to the concentration of adsorbed oxygen in the sample or other vacancy concentration reduction. The sample S3 shows that the highest emission intensity is mainly due to the formation of pure phase $CoWO_4$ at 600°C, and the oxygen vacancy concentration and adsorption oxygen concentration in the sample are at the highest level. In the final analysis, the photoluminescence performance of $CoWO_4$ is affected by impurity concentration, intermediate product concentration, adsorption oxygen concentration, crystallinity and other factors in the sample.

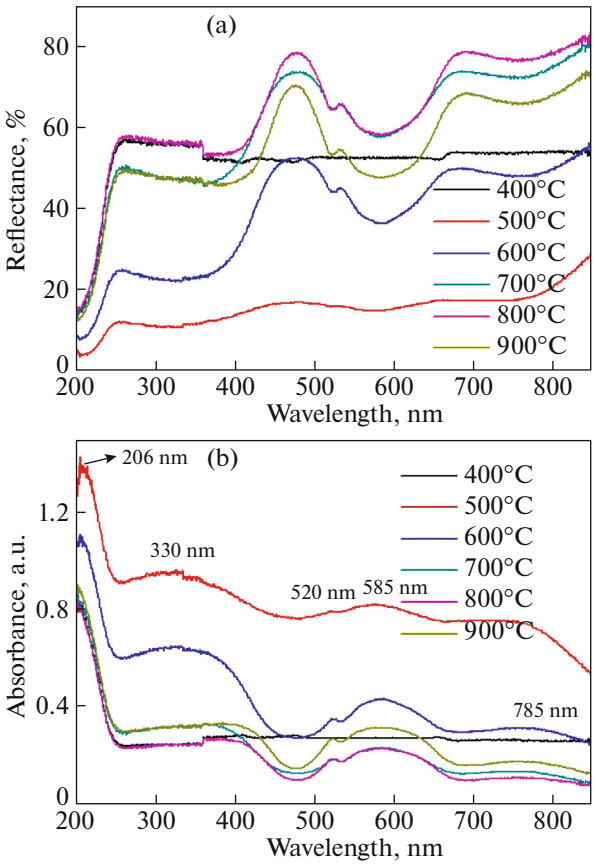


**Fig. 4.** (a) UV–Vis diffuse reflectance spectra and (b) UV–Vis absorption spectra of samples S1, S2, S3, S4, S5, and S6.

The Commission Internationale de l'Eclairage (CIE) diagram of samples S1, S2, S3, S4, S5, and S6 under 220 nm xenon lamp excitations have been analyzed by CIE 1931 software. The CIE color coordinates ($x$, $y$) of samples S1, S2, S3, S4, S5, and S6 were found to be (0.1387, 0.1053), (0.1178, 0.3086), (0.1337, 0.1767), (0.1257, 0.1768), (0.1193, 0.1326), and (0.1272, 0.1459), respectively. The luminescence of $CoWO_4$ is mainly concentrated in the blue-green area. The $CoWO_4$ phosphor has potential application in the field of blue-green light emission.

It can be seen from the calculation in Table 1 that the $E_g$ value of $CoWO_4$ is very large ($E_g$ = 5.191 eV), and only excitation under ultraviolet light can make the electron transition from valence band to conduction band. According to literatures [8, 31], the $(WO_6)^{6-}$ levels consist of ground state $^1A_{1g}$ and the

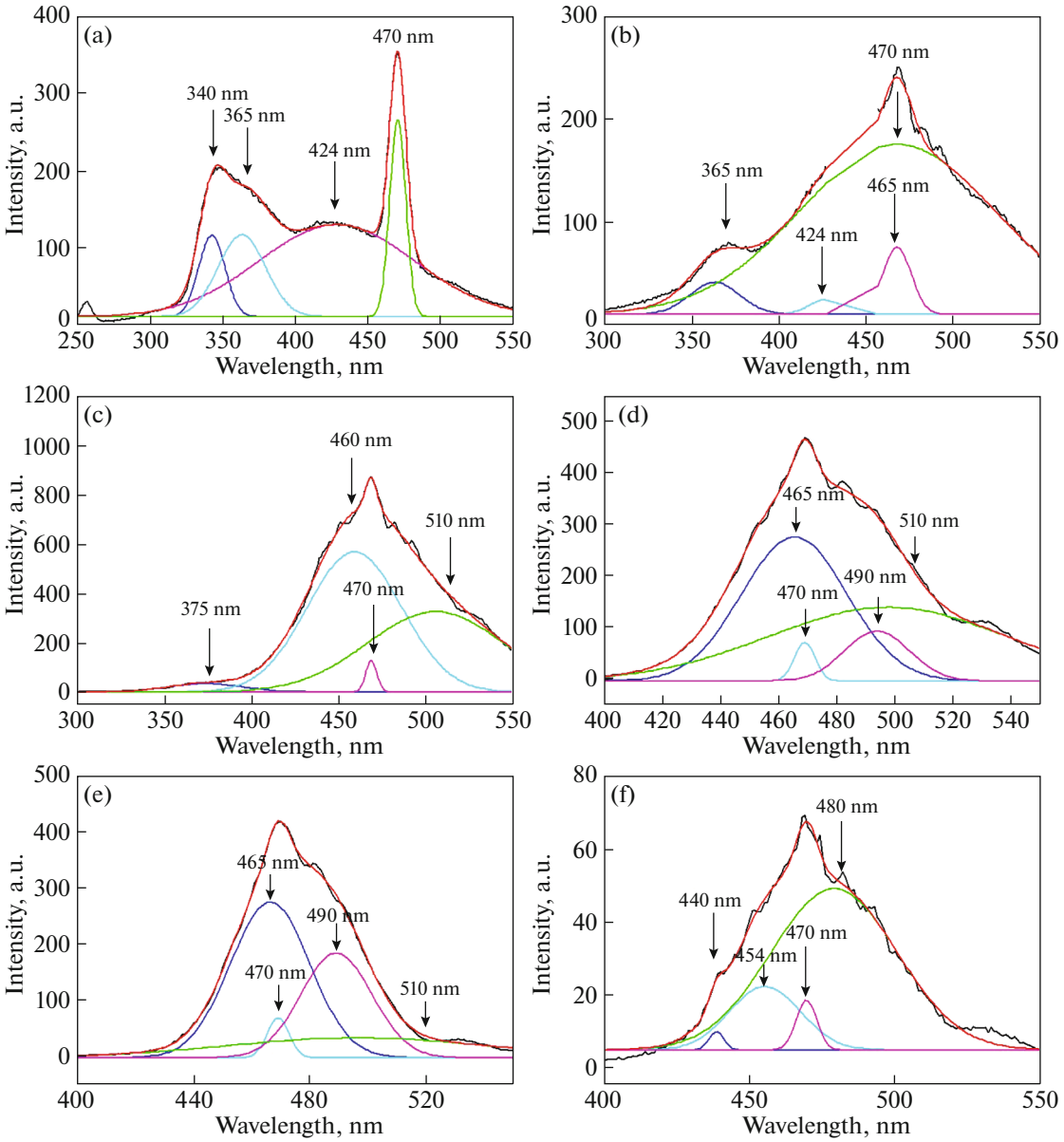


**Fig. 5.** Emission spectrum of samples: (a) S1, (b) S2, (c) S3, (d) S4, (e) S5, and (f) S6 with the excitation wavelength at 220 nm.

excited state $^3T_{1g}$, $^1T_{1g}$, $^3T_{1u}$, $^1T_{1u}$. When the 220 nm light is used to excite the $CoWO_4$ phosphor, the electrons transition from the ground state to the excited state. Due to the presence of organic impurities in the sample, the transport of electrons from the ground state to the excited state is promoted, and ultraviolet luminescence (340–375 nm) is generated during the process of recombination with the holes left by the ground state under the action of vibration relaxation. The blue light emission (424–490 nm) can be ascribed to the transition of $^3T_{1u}$ levels to the $^1A_{1g}$ level. Generally, the spin transition of $T_{1g}$ to $^1A_{1g}$ is forbidden. However, this transition is partially allowed due to the spin orbit coupling, resulting in a green light emission peak at 510 nm in $CoWO_4$.

### *Supercapacitive Performance*

In order to study the influence of different sintering temperatures on the electrochemical properties of $CoWO_4$, the cyclic voltammetry (CV) curve of samples (a) S1, (b) S2, (c) S3, (d) S4, (e) S5, and (f) S6 measured at the scan rates of 5, 10, 50, 100, and 200 mV $s^{-1}$ in the potential range of 0–0.4 V are shown in Fig. 6. For the all samples, the specific current increased with the increasing of the scan rate. The anode and cathode peaks of samples (a) S1, (b) S2,

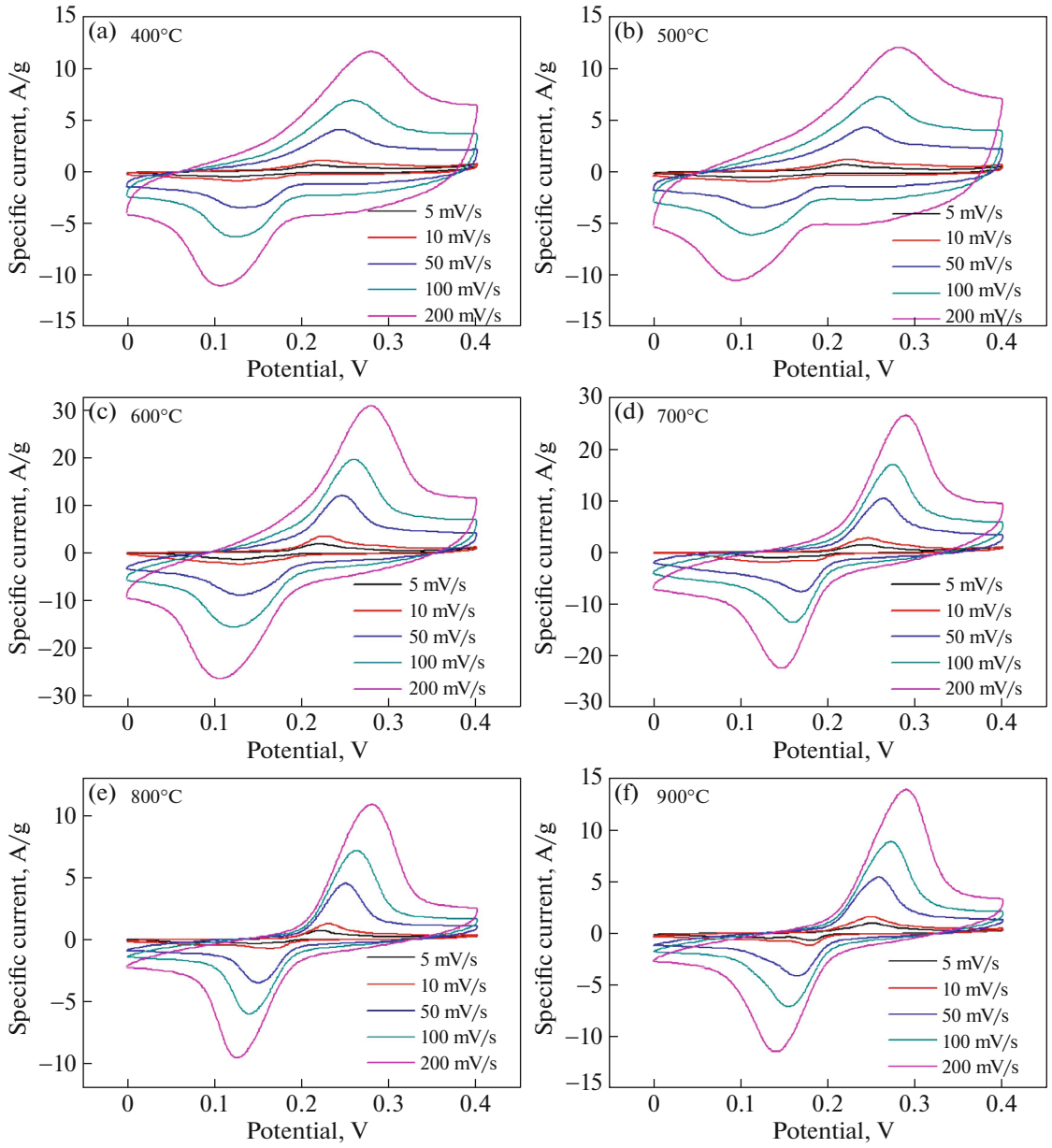


**Fig. 6.** Cyclic voltammograms of samples: (a) S1, (b) S2, (c) S3, (d) S4, (e) S5, and (f) S6.

(c) S3, (d) S4, (e) S5, and (f) S6 move towards lower potential and higher potential respectively with the increasing of scan rate. It can also be seen from the figure that organic impurities and $WO_3$ have a great influence on the shape of CV curve of $CoWO_4$ powder. With the improvement of the phase purity of $CoWO_4$ powders, the CV curve middle region narrowed. The sample S2 have a maximum integrated area in CV curve than that of other samples, suggesting that the sample possess highest electrochemical performance. Combining Fig. 5 and electrochemical performance analysis results, it can be seen that there is some correlation mechanism between $CoWO_4$ photoluminescence and supercapacitor performance. This internal correlation mechanism is still unclear and needs further study.

## CONCLUSIONS

In summary, the cobalt tungstates nanoparticles with special defect structure has been successfully prepared via GIAPGM, which is an excellent phosphor withe high photoluminescence and supercapacitor properties. The sintered samples were characterized by XRD, XPS, SEM, TEM, UV–Vis, PL, and electrochemical workstation. The results indicate that the phase purity and crystallinity of $CoWO_4$ increases with

the increasing of sintering temperature. Color, optical, photoluminescence, and electrochemical properties demonstrate strong temperature dependent behavior. The photoluminescence emission bands at 340–375, 424–490, and 510 nm can be assigned to the organic impurities, the transition of $^3T_{1u}$ levels to the $^1A_{1g}$ level, and the partially allowed transition of $T_{1g}$ to $^1A_{1g}$, respectively. Based on the molecular orbital theory, a reasonable photoluminescence mechanism of $CoWO_4$ phosphor is proposed. The electrochemical properties indicating that the $CoWO_4$ is a promising supercapacitor for advanced electrochemical energy storage applications. Additionally, the current GIAPGM is valuable for preparing other phosphors or supercapacitors with special defects.

## CONFLICT OF INTEREST

The authors declare that they have no conflict of interest.

## ACKNOWLEDGMENTS

This work was supported by the NSAF joint Foundation of China (U2030116), the Chongqing Natural Science Foundation (cstc2019jcyj-msxmX0310), project 2019DB02 supported by NPL, CAEP, the Talent Introduction Project (09924601), the Science and Technology Research Program of Chongqing Education Commission of China (KJZD-K202001202, KJQN201901, KJQN202001225).

## REFERENCES

1. Y. Chen, S. W. Park, B. K. Moon, B. C. Choi, J. H. Jeong, and C. Guo, CrystEngComm **15**, 8255 (2013).
2. Y. Wang, S. F. Wang, X. Y. Yu, S. N. Tang, S. B. Han, and L. Yang, Optik **210**, 164508 (2020).
3. S. F. Wang, Y. Wang, H. J. Gao, J. Y. Li, L. M. Fang, X. L. Yu, S. N. Tang, X. X. Zhao, and G. Z. Sun, Optik **221**, 165363 (2020).
4. M. Golkari, H. Shokrollahi, and H. Yang, Ceram. Int. **46**, 8553 (2020).
5. J. Wang, Z. J. Zhang, J. T. Zhao, H. H. Chen, X. X. Yang, Y. Tao, and Y. Huang, J. Mater. Chem. **20**, 10894 (2010).
6. M. R. Khalifeh, H. Shokrollahi, S. M. Arab, and H. Yang, Mater. Chem. Phys. **247**, 122838 (2020).
7. H. J. Gao, X. X. Zhao, H. M. Zhang, J. F. Chen, S. F. Wang, and H. Yang, J. Electron. Mater. **49**, 5248 (2020).
8. M. Jeyakanthan, U. Subramanian, and R. B. Tangsali, J. Mater. Sci. Mater. Electron. **29**, 1914 (2018).
9. S. T. Guan, R. S. Li, X. F. Sun, T. Xian, and H. Yang, Mater. Technol. **36**, 603 (2021). https://doi.org/10.1080/10667857.2020.1782062
10. V. B. Mikhailik, H. Kraus, V. Kapustyanyk, M. Panasyuk, Y. Prots, V. Tsybulskyi, and L. Vasylechko, J. Phys. **20**, 365219 (2008).
11. Q. Q. Duan, J. Y. Jia, X. Hong, Y. C. Fu, C. Y. Wang, K. Zhou, X. Q. Liu, H. Yang, and Z. Y. Wang, Sol. Energy **201**, 555 (2020).
12. S. Zhang, L. Lv, H. Wang, C. Zhu, R. Pang, J. Feng, and C. Li, J. Lumin. **211**, 183 (2019).
13. S. R. Lu, L. Xia, J. M. Xu, C. H. Ding, T. T. Li, H. Yang, B. Zhong, T. Zhang, L. N. Huang, L. Xiong, X. X. Huang, and G. W. Wen, ACS Appl. Mater. Interfaces **11**, 18626 (2019).
14. S. Wang, H. Gao, G. Sun, Y. Li, Y. Wang, H. Liu, C. Chen, and L. Yang, Opt. Mater. **99**, 109562 (2020).
15. P. Taneja, S. Sharma, A. Umar, S. K. Mehta, and S. K. Kansal, Mater. Chem. Phys. **211**, 335 (2018).
16. U. Subramanian, S. J. Naik, R. B. Tangsali, and A. V. Salker, J. Lumin. **134**, 464 (2013).
17. S. Thongtem, S. Wannapop, and T. Thongtem, Ceram. Int. **35**, 2087 (2009).
18. S. Wang, D. Li, C. Yang, G. Sun, J. Zhang, Y. Xia, C. Xie, G. Yang, M. Zhou, and W. Liu, J. Sol-Gel Sci. Technol. **84**, 169 (2017).
19. H. J. Gao, H. Yang, and S. F. Wang, J. Sol-Gel Sci. Technol. **86**, 206 (2018)
20. S. Tang, S. Wang, X. Yu, H. Gao, X. Niu, Y. Wang, X. Zhao, G. Sun, and D. Li, Chem. Sel. **5**, 10599 (2020).
21. S. Wang, H. Gao, G. Sun, Y. Wang, L. Fang, L. Yang, L. Lei, and Y. Wei, Russ. J. Phys. Chem. A **94**, 1234 (2020).
22. S. Wang, H. Gao, G. Sun, J. Zhang, Y. Xia, C. Xie, G. Yang, Y. Wang, and L. Fang, J. Clust. Sci. **32**, 569 (2021). https://doi.org/10.1007/s10876-020-01815-6
23. S. Wang, H. Gao, X. Yu, S. Tang, Y. Wang, L. Fang, X. Zhao, J. Li, L. Yang, and W. Dang, J. Mater. Sci. Mater. Electron. **31**, 17736 (2020).
24. J. M. Ferreira, J. W. M. Espinosa, M. A. Maurera, E. Longo, P. S. Pizani, I. Garcia, and A. G. Souza, in *Proceedings of the ISMC 11th International Conference on Advanced Materials, Rio de Janeiro, Brazil, 2009.*
25. S. V. Green, A. Kuzmin, J. Purans, C. G. Granqvist, and G. A. Niklasson, Thin Solid Films **519**, 2062 (2011).
26. S. Wang, H. Gao, Y. Wei, Y. Li, X. Yang, L. Fang, and L. Lei, CrystEngComm **21**, 263 (2019).
27. J. Kim, J. Y. Do, N. K. Park, J. P. Hong, and M. Kang, Sep. Purif. Technol. **207**, 58 (2018).
28. Z. Dohnalová, P. Šulcová, and M. Trojan, Dyes. Pigments **80**, 22 (2009).
29. S. Rajagopala, V. L. Bekenev, D. Nataraj, D. Mangalarajc, and O. Y. Khyzhun, J. Alloys Compd. **496**, 61 (2010).
30. S. Rajagopala, D. Nataraj, O. Y. Khyzhun, Y. Djaoued, J. Robichaud, and D. Mangalaraj, J. Alloys Compd. **493**, 340 (2010).
31. C. Zhang, D. Guo, C. Hu, Y. Chen, H. Liu, H. Zhang, and X. Wang, Phys. Rev. B **87**, 035416 (2013).